Design of experiments to spectroscopically characterize radiation flow in stochastic media

Byvank, Tom; Coffing, Shane Xavier; Lioce, Dominic Andrew; Fryer, Christopher Lee; Fontes, Christopher John; Kozlowski, Pawel Marek; Johns, Heather Marie; Camdzic, Dzafer; Elshafiey, Ahmed Tarief Fawzy; Meyerhofer, David Dietrich; Robey, Harry F. III; Feltman, Jacob Michael; Recamier, Claire Lotus; Barnak, D. H.; Hamilton, Christopher Eric; Edwards, Stephanie Lynn; Love, Kevin Noble; Patterson, Brian M.; Farhi, Barak Yitzhak; Jones, Benjamin Jesse; Cleveland, Jacob William; et al.

To be published in: Physics of Plasmas

DOI to publisher's version: 10.1063/5.0198139

Design of Experiments to Spectroscopically Characterize Radiation Flow in Stochastic Media

T. Byvank,[1, a)] S. X. Coffing,[1] D. A. Lioce,[1] C. L. Fryer,[1] C. J. Fontes,[1] P. M. Kozlowski,[1] H. M. Johns,[1] Dž. Čamdžić,[1] A. T. Elshafiey,[1] D. D. Meyerhofer,[1] H. F. Robey,[1] J. M. Feltman,[1] C. L. Recamier,[1] D. H. Barnak,[2] C. E. Hamilton,[3] S. L. Edwards,[3] K. N. Love,[3] B. M. Patterson,[3] B. Y. Farhi,[3] B. J. Jones,[3] J. W. Cleveland,[3] T. H. Day,[3] T. E. Quintana,[3] C. H. Wong,[3] N. S. Christiansen,[3] D. W. Schmidt,[3] A. K. Prinja,[4] and T. J. Urbatsch[1]
[1)] *Radiation Flow Team, Los Alamos National Laboratory, Los Alamos, NM 87545*
[2)] *Laboratory for Laser Energetics, University of Rochester, Rochester, New York 14623*
[3)] *Target Fabrication Team, Los Alamos National Laboratory, Los Alamos, NM 87545*
[4)] *University of New Mexico, Albuquerque, NM 87106*

(Dated: 16 January 2024)

Precise characterization of experimental radiation flow is required to validate the high energy density physics models, numerical methods, and codes that are used to simulate radiation-hydrodynamics phenomena such as thermal radiation transport in stochastic media. The Cassio code is used to simulate thermal radiation flow through inhomogeneous, stochastic-media-foam configurations containing optically thick clumps dispersed within an optically thin background aerogel. Cassio can model small inhomogeneous problems directly, but most problems require approximations to meet computer limitations on run-times and memory usage. Various examples of these approximations are methods that produce, in one calculation, an ensemble-averaged solution and associated standard deviation; reduced spatial dimensionality with approximate geometries; and full material homogenization with no geometric detail. Cassio simulations are used to design experiments at the OMEGA-60 Laser Facility that can measure the radiation flow using the spatially-resolved COAX absorption spectroscopy diagnostic. The experimental platforms flow radiation through foam targets ranging from a background-only aerogel, to a single configuration of a specified stochastic medium, to a fully homogenized foam of the background and clump materials. Under constant total clump mass, larger clumps (here, larger than 10 μm diameter) will mix more slowly with the background such that the bulk radiation flow is faster than it would be in a fully homogenized material. The COAX platform can be used to infer temperature and density profiles in both the background material and clumps, simultaneously, and therefore to differentiate radiation flow in a range of stochastic and homogeneous media.

I. INTRODUCTION

High Energy Density Physics (HEDP) experiments[1–5] are a mid-scale avenue for validating radiation hydrodynamics codes, the underlying physical data used by the codes, the numerical methods embodied in the codes, and the approximations necessary to make code execution tractable.

Radiation hydrodynamics numerical simulations of large-scale problems such as supernovae and other astrophysical phenomena[6–8], helioseismology[9–11], atmospheric imaging[12–14], nuclear reactors[15,16], oncological treatments[17], radiation shielding[18,19], animated films[20], and HEDP experiments[21–25] remain costly and complicated, especially with the ever-increasing demand for higher fidelity. A dominant expense in these multi-physics simulations is solving the Boltzmann transport equation, whether it is for light rays, neutrons, or thermal x-rays nonlinearly coupled to hot material. Balancing desired accuracy with tractable approximations to the transport solutions in multi-physics simulations is the workhorse for many of these fields. One of those fidelity challenges is transport in stochastic media, in which multiple material components such as dense clumps, differing chemical species, or irregular regions may be dispersed in a background material. Direct multi-physics numerical simulation of large-scale problems is prohibitive in brute force, even for just one of an infinite number of realizations of the stochastic media distribution, to obtain the average solution plus its standard deviation. The most straightforward approximation to stochastic media is full spatial homogenization, wherein the material is treated as a spatially uniform mixture. However, homogenization incorrectly decreases the photon mean free path and produces inaccurate transport solutions, especially as the optical depths of the materials becomes increasingly disparate.

For over half a century[26], methods have been under development to solve for the average solution of a transport-in-stochastic-media problem[27–41], with most development for binary Markovian mixtures. The Levermore-Pomraning method[42] involves solving a transport equation for each material with a closure term containing the average chord lengths in each individual material. The average is derived from the distribution of chord lengths from randomly sampled initial locations and angular orientations in an individual material. Much of the methods development has been for linear transport, particularly neutrons, with

[a)] tbyvank@lanl.gov

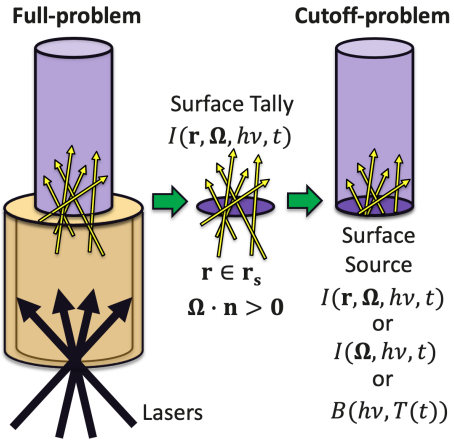

FIG. 1. (Left) The full-problem simulation uses laser ray tracing (black arrows) to model the halfraum (gold) heating and radiation flow (yellow arrows) into the foam tube (purple). (Middle) A surface tally in the full-problem between the halfraum and foam tube records the intensity that can be used as a surface source for a subsequent (Right) cutoff-problem containing only the foam tube.

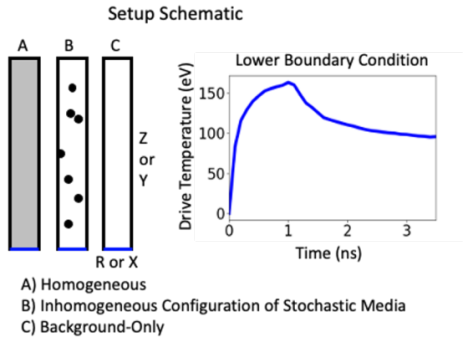

FIG. 2. (Left) Cutoff-simulation schematic of foam materials: A) homogeneous uniform distribution of all particles, B) stochastic media of optically thick clumps within an optically thin background, C) the optically thin background-only material. Radiation propagates in the axial direction (Z or Y), with the origin at the lower boundary. (Right) Radiation drive profile vs. time applied at the simulation lower boundary (sending a radiation flow upward into the foam), peaking at 160 eV at 1 ns.

some study of thermal x-ray transport. Radiation-hydrodynamics development[43–45] has evolved without commensurate hydrodynamics methods for stochastic media. To study radiation-hydrodynamics transport-in-stochastic-media, both effects must be modeled together.

Recent developments providing more detailed and spatially-resolved spectral diagnostics[46] have made HEDP experiments attractive for validating transport-in-stochastic-media ensemble-solution methods. Replicate experiments can probe the numerical and theoretical distribution of solutions, and a well-characterized and well-diagnosed single experiment can validate several of the underlying attributes of radiation hydrodynamics such as: transport across interfaces, spectral and spatial averaging of opacities, spatial discretizations, time-implicitness methods, reduced dimensionality, operator split algorithms, equations of state, and completeness of physics. Modeling an HEDP experiment in 3D with sufficient phase-space resolution is still challenging, but possible, on modern supercomputers.

In this work, we consider stochastic media that are binary mixtures of optically thick particulates (clumps) dispersed within an optically thin substrate (background). Clumps may have various size and spatial distributions. For any nominal configuration of a stochastic media, the specific location of a clump cannot be determined. Modelers must develop an average solution and standard deviation for any configuration to encompass any likely variation of radiation flows through stochastic media. Radiation hydrodynamics through a stochastic media can be different than the radiation flow in an atomically-mixed homogeneous material wherein the same total number of particles (relative to the clumps and background particles in the stochastic media) are uniformly distributed. Here we focus on the detailed diagnosis of a single HEDP experimental configuration. For a single inhomogeneous foam, a CT scan[47] can characterize the size distribution and spatial locations of inclusions and background materials, providing initial conditions for simulations that resolve the constituent materials. We expect these experimental results to advance the validation of transport-in-stochastic-media methods beyond the current state of the art.

The present research considers radiation propagating through a foam tube that is either an inhomogeneous configuration of a stochastic media or a homogeneous configuration (comparable to foams in prior experiments[48–51]). The inhomogeneous configuration consists of V_2O_5 optically thick clumps in a $(Sc_2O_3)(SiO_2)_4$ optically thin aerogel background[52,53]. The radiation drive is generated using the OMEGA-60 Laser Facility to heat a halfraum (Au can) which sends a transonic Marshak wave into the attached foam tube. Radiation flow can be characterized by breakout measurements[54] and radiography[55–57] of hydrodynamic shocks. For a more-detailed measurement that better constrains simulation predictions, the COAX platform[48–51] on OMEGA provides spatially-resolved absorption spectroscopy data (± 8 eV temperature precision, ± 23 μm spatial resolution over a 760 μm extent).

The paper is organized as follows. Section II de-

scribes our modeling tool, the Cassio code, and how we model simulations of the experimental configurations. Section III discusses the design simulations of the initial OMEGA experiments. Section IV presents preliminary data from the initial experiments. Section V examines a simulation scan of clump sizes and their effects on radiation flow in stochastic media. Section VI explores additional aspects of the stochastic media radiation flow research. Conclusions are presented in Sec. VII.

II. SIMULATION SPECIFICATIONS

For all simulations in this work, we use the Eulerian, Adaptive Mesh Refinement (AMR), radiation hydrodynamics code, Cassio[58,59]. These Cassio simulations are 2T, with different possible material temperature and radiation temperature but the same (material) temperature for electrons and ions. The tabulated SESAME equation of state (EOS) for the background $Sc_2Si_4O_{11}$ aerogel is modeled as SiO_2 with porosity to set the density. The V_2O_5 clumps are similarly modeled with a porous V EOS. Different choices for EOS models influence the radiation flow dynamics but are outside the scope of the present design study. We set correct densities using available materials that contain the dominant elements present in the true materials. Implementation of the correct equation of states for the true oxides and mixtures requires a detailed study to validate modeling choices.

The radiation flow is modeled with Multi-Group Implicit Monte Carlo (MG IMC) radiation transport using 71 photon energy bins with tabular opacity data from the Los Alamos OPLIB opacity database[60–62]. Material opacities for individual components are atomically-mixed using the TOPS code (`http://aphysics2.lanl.gov/opacity/lanl`). For the inhomogeneous foam configurations, where the clumps are modeled explicitly in space, the aerogel background and clump materials have their own atomically mixed opacities. Within a computational spatial cell containing multiple components, Cassio maintains total pressure equilibrium between the components. Spatial cells are used to explicitly resolve individual clumps, but cells containing interfaces will necessitate atomic mixing of all constituent materials. For atomically-mixed cells, Cassio mixes the opacities of the components based upon their mass fraction in the cell.

For the OMEGA experiment, the foam is a 900 μm-diameter, 2000 μm-high cylinder. Modeling the entire foam tube and laser-heated halfraum is tractable in 2D RZ geometry but computationally expensive due to the laser ray tracing. A common approximation is to run just the foam tube as a cutoff-problem, using a drive obtained from a full-problem simulation, as shown in Fig. 1. The full-problem calculation uses laser ray tracing to model the halfraum heating. That computational cost is reduced by tallying the radiation across a surface between the hohlraum and foam tube, capturing the intensity I as a function of location r (on surface r_s with normal direction n), angle Ω, energy hν, and time t. The intensity from the surface tally can then be used as a source for subsequent cutoff-problems with only the foam tube. The cutoff drive – the surface source – may be approximated further by integrating out location on the surface, the angle, and/or taking the energy profile to be a blackbody, B(hν,T(t)), with radiation temperature T.

For the inhomogeneous media considered here, even a cutoff problem can be too expensive, so here a smaller portion of the foam tube is modeled. The experimental configuration here is modeled in 2D cylindrical (RZ) coordinates in Sec. III at a maximum spatial resolution of 4 μm with vacuum boundary conditions at the outer-R and top and bottom ($\pm Z$) boundaries. For the design parameter scan in Sec. V, a small section of the foam is modeled in a 112 μm $\times$ 800 μm Cartesian (XY) geometry at a 0.25 μm spatial resolution with reflecting boundary conditions at the left and right boundaries and vacuum boundary conditions at the top and bottom boundaries. For all simulations, a time-dependent radiation temperature drive, obtained from a higher-fidelity, full-problem simulation, is approximated on the bottom boundary as an effective blackbody source. As illustrated in Fig. 2, the drive has a 160 eV peak radiation temperature at 1.0 ns. By modeling the radiation temperature drive as only an isotropic blackbody in local-thermodynamic-equilibrium (LTE), information is lost about the frequency-dependent spectra and angle of the drive (not a pure blackbody) as well as any non-LTE conditions present. By simplifying the drive, the computational time is reduced for parameter scans that build intuition about the radiation flow dynamics.

Inhomogeneous configurations are initialized by placing 2D disks of clump material (3.357 g/cc V_2O_5) at a desired volume fraction within a background ($Sc_2Si_4O_{11}$ at 120 mg/cc in Sec. III and 60 mg/cc in Sec. V); see Fig. 2 (B). For cylindrical simulations the clump disks become toroids, and for Cartesian simulations the clump disks become infinite rods; in the present work, the key feature is the clump volume fraction (or 2D area fraction)– the volume taken by the clumps divided by the total foam volume. The clump locations are determined by a random uniform probability distribution, and clumps are not allowed to overlap. In the present simulation design work, the clump diameter is set to be constant for a given configuration, but there can be a distribution of clump sizes in fabricated foam targets for experiments. Based on an analysis of chord length distributions for the initial setups of inhomogeneous configurations, the background is largely Markovian (an exponential chord length distribution), although modified due to a finite system domain size, while the clumps are not Markovian but have a well-defined chord length distribution[63].

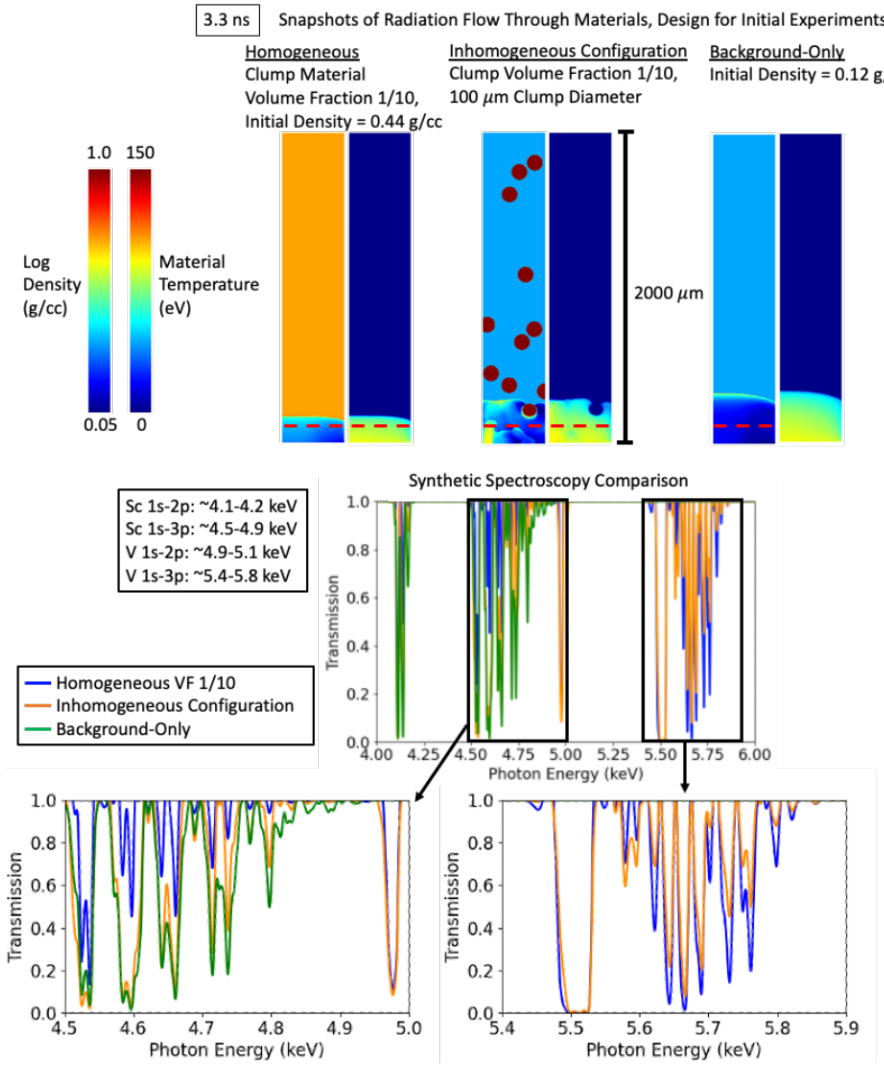

FIG. 3. (Top) Pairwise plots of density (left) and material temperature (right) at 3.3 ns of the radiation flow traveling through various foam configurations: homogeneous foam with a clump volume fraction VF = 1/10, an inhomogeneous configuration with the same VF = 1/10, and a background-only foam. Radiation is traveling upward, and the left boundary is the cylindrical axis of symmetry. (Bottom) Synthetic spectroscopy from post-processed simulation outputs from the lineouts (red horizontal dashed lines). Note the different spectroscopy signals for the various foam configurations, which demonstrates how the spectroscopy diagnostic can be used to differentiate among the various foam configurations and simultaneously measure conditions of both the optically thick clumps (V-lines) and optically thin background (Sc-lines).

Spectral post-processing of the simulation outputs permits investigation of how the COAX spectral diagnostic can discriminate between radiation flow in stochastic media and homogeneous materials. In the present

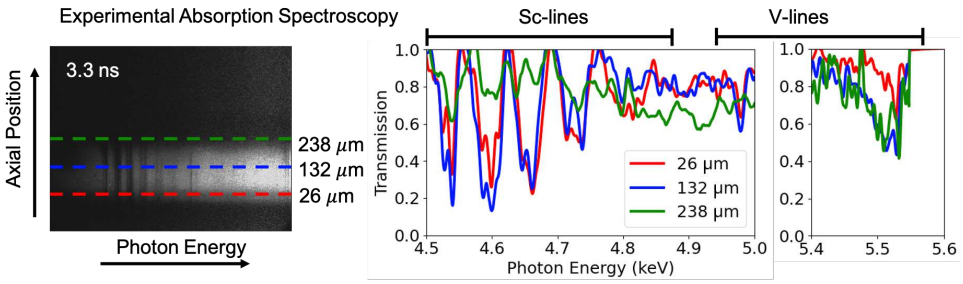

FIG. 4. Experimental spectra of a stochastic media foam configuration from OMEGA shot 104186. At multiple axial positions above the lower foam boundary (lineouts shown for 3 example heights), measurements are obtained of both the clumps (V-lines) and background (Sc-lines) materials.

work, the foam configurations are designed to permit simultaneous absorption spectroscopy measurements of both the clumps (V-lines) and background material (Sc-lines). These detailed experimental measurements can support validation and further development of numerical methods in radiation hydrodynamics codes.

III. SIMULATION DESIGN OF INITIAL EXPERIMENTAL CONFIGURATION

The first design goal for these experiments is to extend the COAX temperature diagnostic to use absorption spectroscopy simultaneously on both the clumps (V-lines) and background material (Sc-lines) to characterize the radiation flow propagating through the inhomogeneous configuration of a stochastic media.

Inhomogeneous foams are generated with 3.357 g/cc V_2O_5 100 μm-diameter clumps at a $\sim$1/10 volume fraction placed in a 120 mg/cc $Sc_2Si_4O_{11}$ background. The overall density is 0.44 g/cc. Homogenizing this foam would have uniformly distributed V_2O_5 (86.6% atomic fraction) within the $Sc_2Si_4O_{11}$ (13.4% atomic fraction). The gray Rosseland mean opacity at 125 eV is 3050 cm^2/g for the clumps (1 μm mean free path), 1670 cm^2/g for the background (50 μm mean free path), and 2210 cm^2/g for the corresponding homogenized material (10 μm mean free path).

The qualitative radiation flow dynamics through the foam are as follows. The initially supersonic radiation wave heats and ionizes the foam material. A rarefaction wave follows, propagating at the sound speed. As the halfraum drive cools, the radiation flow decelerates, and the rarefaction wave reaches the radiation front where increasing material pressure ablates material and generates a hydrodynamic shock that passes the now-subsonic radiation front. When the foam is an inhomogeneous media, the radiation travels more easily in the optically thin background than in the optically thick clumps. The radiation wave heats up the clumps and sends a shock into the clumps that eventually rebounds. The increasing pressure causes the clumps to expand and decrease in density. The clump surface closest to the radiation drive heats up and ablates first, before the radiation reaches the opposite side of the clump. Further discussion of the radiation flow and hydrodynamics is presented in Sec. V.

As illustrated in Fig. 3, the bulk radiation flow speed in the inhomogeneous configuration is faster than in the homogenized material. Radial lineouts (red dashed lines in Fig. 3) of the density and temperature at a 100 μm axial height are post-processed by ray-tracing (including monochromatic material absorption and self-emission) to obtain a synthetic absorption spectroscopy transmission signal. Although line saturation (zero transmission) is not seen in the experimental data (Sec. IV), which can occur from full absorption through large inclusions and from incorrect spatial averaging when post-processing the simulation, we can still qualitatively see what absorption lines are predicted by simulation. Overall, the synthetic spectroscopy depicts differences among the signals for the various foam configurations. For this inhomogeneous configuration, simulations predict that the experimental spectral diagnostic can successfully measure spectroscopy of both the clumps (V-lines) and background (Sc-lines) at an example time of 3.3 ns from the beginning of the drive (consistent with the experimental results discussed in Sec. IV).

IV. INITIAL EXPERIMENTAL RESULTS

As detailed in prior work[49], the COAX experimental platform uses a Kr-capsule backlighter to provide a broadband source, and absorption spectra are collected for photon energies between 4.5 to 5.6 keV with 3.8 eV resolution. Future work will extend the photon energy range to collect more data on V-lines. The COAX diagnostic on OMEGA provides spatially-resolved absorption spectroscopy data with $\pm$8 eV temperature precision and

± 23 μm spatial resolution over a 760 μm field-of-view, dependent upon magnification.

Figure 4 shows experimental spectra from the HEDP experiment OMEGA shot 104186 from the XFOL campaign (a follow-on to the COAX platform), at 3.3 ns (with 0.2 ns integration time) relative to the beginning of the 1 ns square laser pulse. Spectra are obtained at multiple axial heights above the lower foam boundary (lineouts shown for 26 μm (red), 132 μm (blue), 238 μm (green)), line-integrated across the foam diameter. Background calibration is accounted for by taking a separate spectral measurement (not shown) of the backlighter source and fitting the continuum. The different plasma temperature and density conditions at different heights lead to different resulting spectra. This experiment successfully simultaneously measures spectral lines from both the clumps (V-lines) and background (Sc-lines) material, which permits diagnosing the plasma conditions of both materials as the radiation flow travels through the inhomogeneous foam.

The experimental configuration consists of radiation traveling through an inhomogeneous foam with similar material compositions as described in Sec. III. For these initial experiments, foams were fabricated by introducing $\sim$1 μm diameter V_2O_5 particles into an aerogel matrix made of $(Sc_2O_3)(SiO_2)_4$. The $\sim$1 μm particles aggregate into larger-sized clumps with a distribution of sizes from less than 5 μm to greater than 200 μm. Based on comparing the analysis of related foams in the same production batch, estimated foam specifications are a $\sim$1/10 volume fraction of the 3.3 g/cc clumps within the 120 mg/cc background aerogel.

In qualitatively comparing the synthetic spectra in Fig. 3 and the experimental spectra in Fig. 4, simulations and experiments each show both Sc-lines and V-lines. The quantitative transmission is different, with the synthetic spectra predicting less transmission because of absorption through a 100 μm diameter clump at the shown lineout height. Future efforts will investigate the radiation flow conditions predicted by the Cassio code compared to the experimentally observed spectroscopy, using detailed initial conditions of the foam configuration as measured with a CT scan, which includes a distribution of clump sizes and shapes. A more quantitative analysis of relative lines ratios and shapes will provide time-resolved data on the temperatures, densities, and ionization states of both the clumps and background materials. For the purpose of the present work, we again qualitatively highlight that the simulations (Fig. 3) and experiments (Fig. 4) each depict successful spectroscopic measurements of both the clump (V-lines) and background (Sc-lines) materials.

V. DESIGN SCAN OF STOCHASTIC MEDIA EFFECTS

Radiation dynamics are explored numerically through inhomogeneous foams with varying clump sizes (2, 5, 15, and 30 μm diameters), homogeneous foams of a uniform material with the same amount of clump material as in the stochastic inhomogeneous configurations, and background-only foams with no clumps. As observed in prior research of inhomogeneous configurations with clump diameters below $\sim$10 μm, the radiation flow quickly heats the clumps and causes the clumps to mix with the background, leading to behavior like a homogeneous foam with the same total component mass[48]. For diameters greater than $\sim$10 μm, the clumps do not fully atomically-mix with the background, and the radiation flow in the inhomogeneous media behaves similarly to the radiation flow in a background-only foam that is spatially-modulated by the optically thick clumps. The "critical" $\sim$10 μm clump size is based on the transition between the limits of atomic mix and chunk mix for an effective opacity[33], which occurs when the clump size di-

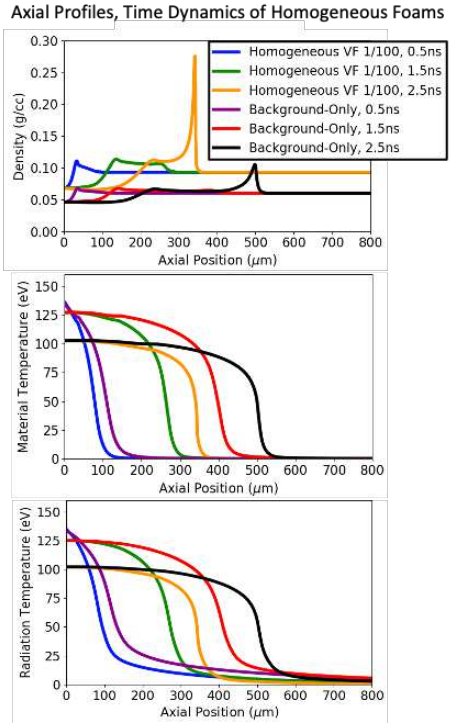

FIG. 5. Axial profiles (along the Z or Y direction) of density, material temperature, and radiation temperature at various times (0, 1.5, and 2.5 ns) for a homogeneous foam with a clump volume fraction VF = 1/100 (blue, green, orange) and a background-only foam (purple, red, black). Note the time development of a density spike at later times as the radiation front propagates and temperature decreases.

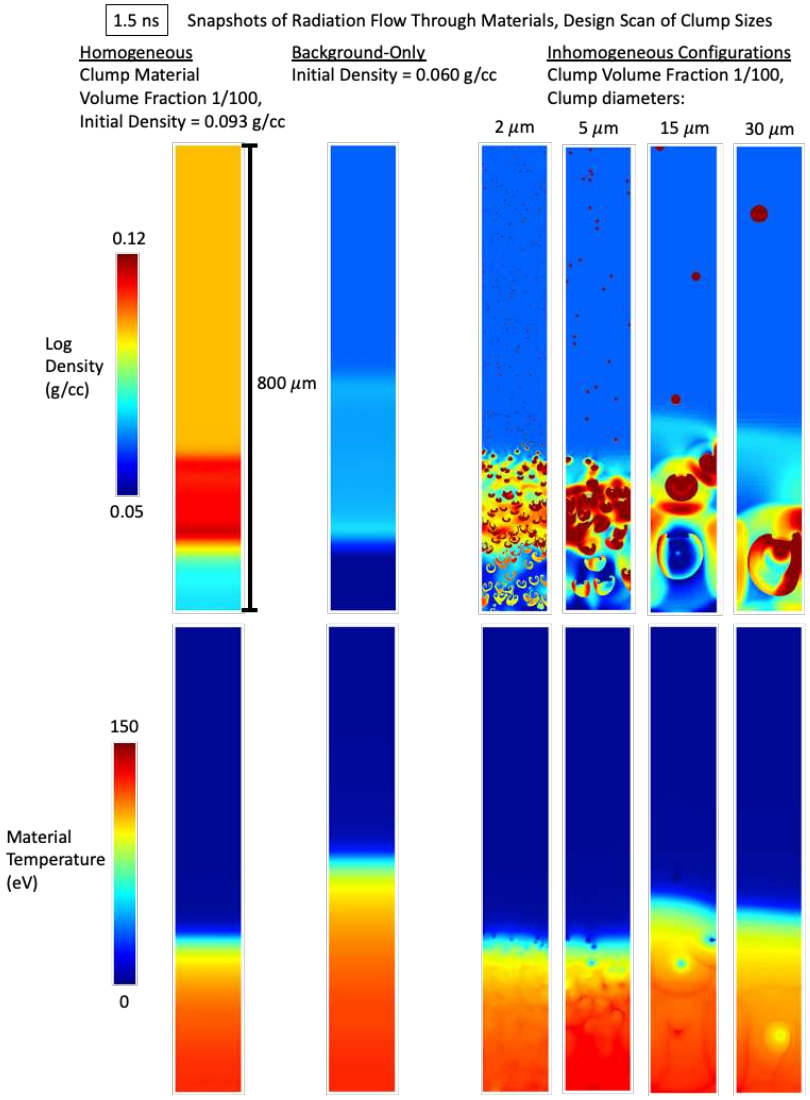

FIG. 6. At 1.5 ns, images of density (Top) and material temperature (Bottom) for various foam configurations: homogeneous (Left), background-only (Middle), and inhomogeneous configurations with different clump sizes (4 Right). Note the radiation flow in the 2 μm and 5 μm clump diameter inhomogeneous foams behave similarly to the homogeneous foam, while the radiation flow in the 15 μm and 30 μm diameter foams behave similarly to a modulated background-only foam.

vided by the clump photon mean free path ($\sim$1 μm, see the following paragraph) is approximately equal to 10.

To better constrain simulation predictions, more axially-resolved spectroscopy data are desired over the available 760 μm spatial extent of the COAX diagnostic spectroscopy measurement (see the limited spatial information in the Fig. 4 image not covering the full axial extent of the detector). Taking measurements at a

later time can provide some of this data, but later times have lower temperatures as the radiation wave cools, which can degrade the spectroscopy signal because less-ionized (cold) material leads to less-prominent absorption spectroscopy peak features (closer to background transmission levels). The axial extent of radiation flow increases with decreasing foam density and the corresponding amount of material needing to be ionized. In the Cassio simulations in the present section, the background density is reduced to 60 mg/cc and the clump volume fraction is reduced to 1/100, giving an average total foam density of 93 mg/cc. In this situation, the Rosseland mean (gray) opacity at a 125 eV temperature is 3050 cm^2/g for the clumps (1 μm mean free path), 1040 cm^2/g for the background (160 μm mean free path), and 1340 cm^2/g for the corresponding homogenized material (80 μm mean free path).

The radiation flow dynamics in homogeneous foams are depicted in Fig. 5 (profiles averaged along the simulation R or X direction). As outlined in Sec. III, as the radiation front propagates axially into the foam, the foam temperature near the drive cools. Eventually, the heated foam material generates a hydrodynamic shock (see the growing density spike in Fig. 5 (Top)). The radiation flows faster in the lower-density and lower-opacity background-only foam relative to the homogeneous foam (clump volume fraction VF = 1/100) consisting of a uniform distribution of V_2O_5 (54.0% atomic fraction) within the $Sc_2Si_4O_{11}$ (46.0% atomic fraction). For a given time, the radiation temperature profile extends farther than the material temperature profile; note the axial locations of the 10 eV radiation temperature vs. 10 eV material temperature.

Figure 6 shows snapshots at 1.5 ns of density and temperature, showing the radiation flow through various foam configurations: homogeneous, background-only, and inhomogeneous configurations with different clump sizes. Below ~10 μm clump diameters in inhomogeneous configurations, the radiation flow quickly heats the clumps and causes the clumps to mix with the background, leading to behavior like a homogeneous foam with the same component masses. In inhomogeneous configurations with clump diameters greater than ~10 μm, the clumps do not fully atomically-mix with the background, and the radiation flow in the inhomogeneous media behaves similarly to the radiation flow in a background-only foam that is spatially-modulated by the optically thick clumps. As the radiation wave encounters the optically thick clumps, shocks are generated and sent through the material. The initially optically thick clumps expand and decrease in density, which reduces their optical thickness as the clumps mix with the background material. This dynamic evolution of the clumps highlights that the present physics study involves radiation-hydrodynamics and transport-in-stochastic-media together rather than "just" transport alone.

In Fig. 7, the axial profiles (along the Z or Y direction, values averaged along the simulation R or X direction) show that the bulk radiation flow for the inhomogeneous configurations with clump diameters greater than 10 μm (blue and black lines) is faster than for the homogeneous foam (green line). For these inhomogeneous configurations, the radiation flow is slower than for the background-only foam (red line), and the relative difference in speed is based upon the precise inhomogeneous configuration. Because at this time the radiation has only traveled about half-way through the foam, the number of randomly placed clumps toward the bottom half in the simulation geometry determine by how much the radiation flow is modulated. An inhomogeneous configuration for which all of the clumps happen to be located in the top quarter of the simulation would have a radiation flow that behaves identically to the radiation flow in the background-only foam.

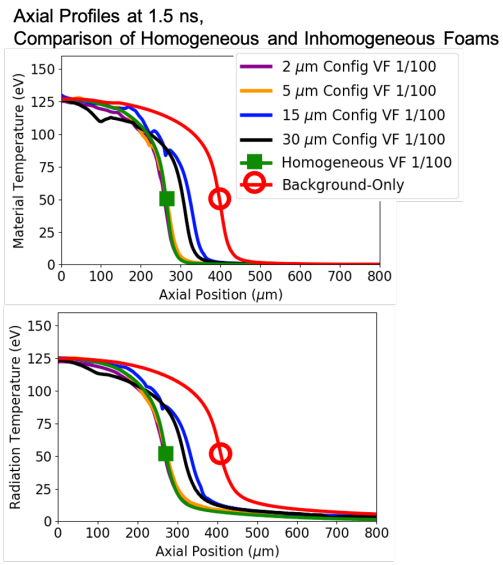

FIG. 7. At 1.5 ns, axial profiles of material temperature (Top), and radiation temperature (Bottom) for various configurations. For the inhomogeneous configurations (purple, orange, blue, black), the optically thick clumps reduce the bulk radiation flow speed through the material, with a lower limit of the speed through the homogeneous foam (green, filled square) and upper limit of the speed through the background-only foam (red, open circle).

Based on the different density, temperature, and material conditions (see Appendix A for plotted profiles), post-processed simulation lineouts predict differences in spectroscopy that help characterize the radiation flow in an inhomogeneous configuration compared to the corresponding homogeneous material or a background-only

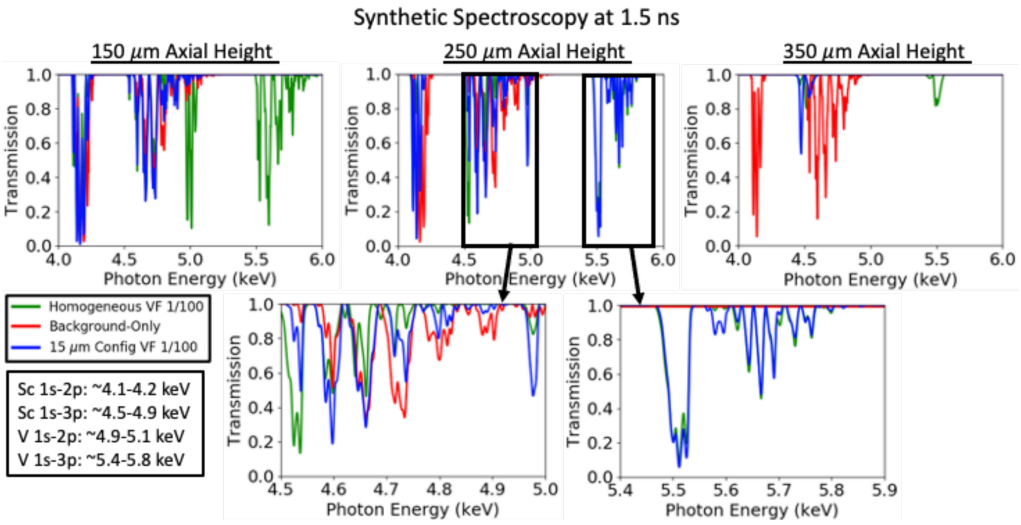

FIG. 8. Synthetic absorption spectroscopy signals post-processed from simulation outputs (radial lineouts along the simulation R or X direction, see Appendix A), displaying differences in spectra at various axial heights (150 μm, 250 μm, 350 μm) for the homogeneous foam (green), background-only foam (red), and inhomogeneous configuration with 15 μm clump diameter (blue). The spatially-resolved ability of the spectroscopy signal to diagnose conditions of the radiation flow allows discrimination between different configurations, which provides a detailed measurement to constrain models.

foam; see Fig. 8. Overall, the main point is that the different foam types lead to different radiation flow and plasma conditions, which therefore creates different resulting spectra. Analysis of relative line shapes permits comparison of the Sc 1s-2p, Sc 1s-3p, V 1s-2p, and V 1s-3p lines, which provides spatially-resolved temperature information for both the $Sc_2Si_4O_{11}$ aerogel background and the V_2O_5 clumps. The spectroscopy is a sensitive diagnostic at temperatures greater than ∼80 eV (dependent on foam density), above which the radiation flow can ionize the electrons into excited states. The spatially-resolved spectroscopy provides information on how far the radiation front has propagated and heated up material; in Fig. 8, the radiation has traveled to 350 μm (above the lower foam boundary with the radiation drive) in the background-only foam but has not yet traveled to that axial extent in the homogeneous foam or inhomogeneous configuration. Vanadium lines are not present in the background-only foam, are always present (above a high-enough temperature) in the homogeneous foam, and are only present in the inhomogeneous foam at heights at which clumps are located (here, at 250 μm, but not 150 μm, above the lower foam boundary with the radiation drive).

Research avenues for future experiments include comparing radiation flow in three types of foams: 1) an inhomogeneous configuration with small clumps less than 10 μm diameter to create behavior similar to a homogenized foam, 2) an inhomogeneous configuration at the same clump volume fraction, with large clumps greater than 10 μm diameter to create a relatively faster radiation flow, and 3) the optically thin background-only foam. Scanning the clump volume fraction can explore effects due to how optically thick or thin the foams are. A notable requirement is that this specified design scan has uniform clump sizes. The additional degree of freedom of a clump-size distribution of clump diameters, with some small and some large, would produced a combination of effects from homogeneous foams and inhomogeneous media. Studying this extra complication is reserved for the future. When foam targets are fabricated for the current campaign, the extent to which clumps aggregate together into larger clumps will be characterized, and a narrow size distribution is desirable.

VI. EXTENSIONS AND FURTHER CONSIDERATIONS

The foam geometry, materials, and radiation drive source can influence how radiation travels through stochastic media and how the radiation interacts with the hydrodynamic development. Advances in target fabrication techniques will permit tailoring of material distributions to desired configurations.

Details of the source that drives the radiation flow influence how the inhomogeneous media modifies the radi-

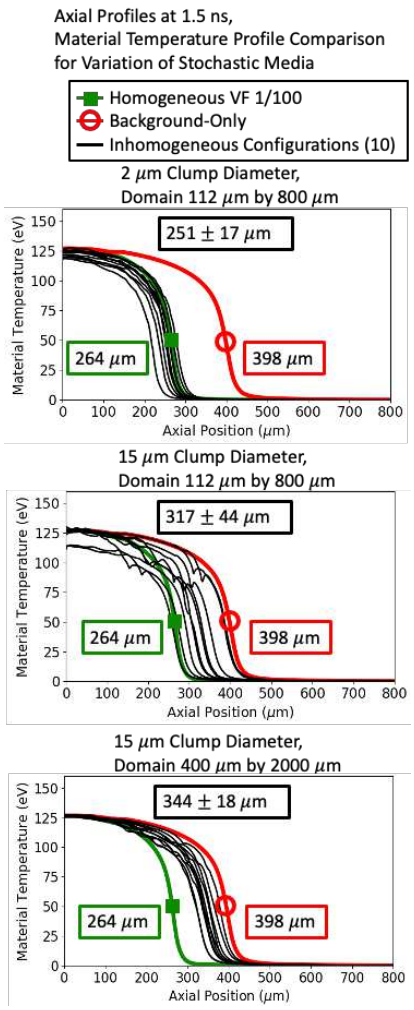

FIG. 9. At 1.5 ns, axial profiles of material temperature comparing radiation flow in ten inhomogeneous configurations (black) with the homogeneous foam (green, filled square) and background-only material (red, open circle). Profiles are compared for 2 μm clump diameter inhomogeneous configurations (Top), 15 μm configurations (Middle), and 15 μm configurations with a larger computational domain size (Bottom). Values in boxes denote the axial locations of a 50 eV material temperature; note the convergence (determined by the standard deviation) of the inhomogeneous configurations.

ation profile. The relatively-low foam densities required for experiments on OMEGA provide a target fabrication constraint that can be addressed by moving the physics platform to the higher-energy National Ignition Facility (NIF)[64]. Conducting experiments on NIF will allow for larger, denser foam targets and investigation of different radiation flow regimes over a larger time span, and this platform development is ongoing in the Xflows campaign[65]. Modifying the radiation source energy changes the relative amount of how optically thick the clumps are relative to the background. At higher energies (and temperatures), the clumps can become optically thinner. Another source modification includes non-LTE sources with non-Planckian spectra. Such a source can affect how particular materials within a stochastic media configuration will change the resultant energy spectra of a propagating radiation wave, which may be different for inhomogeneous media compared to homogeneous foams. The effective drive from the halfraum into an inhomogeneous material could be sensitive to the angular dependence of the radiation initially encountering the clumps.

Numerical transport methods affect the energetics of the radiation hydrodynamics. Use of Implicit Monte Carlo (IMC) transport, discrete ordinates (S_n) transport, or radiation diffusion can influence how the radiation front heats the inclusions, forms shocks at interfaces, and distributes energy within a material. For these methods and by using various foam configurations, future work will explore the time dynamics of how energy is partitioned between radiation energy, kinetic energy, and internal energy of the clump and background materials. The clump ablation rate and mixing time will be examined in relation to timescales for photon transport and hydrodynamics (including material heat capacity effects on ablation), further defining the differences between inhomogeneous configurations with optically thick clumps that are either smaller or larger than 10 μm diameter.

True stochastic media, wherein precise particle locations are not determined, inherently suggest a 3D geometry. Evaluating these 3D effects in relation to 2D setups is the subject of future research, such as whether clump volume fraction is the primary important variable affecting radiation flow dynamics or if other 3D effects (shape, aspect ratio, relative surface area to volume) need to be accounted for. Future work will analyze convergence of how many near direct numerical simulations (that fully resolve the clumps) of particular inhomogeneous configurations are required for data needed to obtain an average solution plus standard deviation for radiation flow through stochastic media. A limited-scope first step in this convergence analysis is shown in Fig. 9, which compares variation among ten inhomogeneous configurations with clump volume fractions VF = 1/100 and either 2 μm or 15 μm clump diameters, in addition to the corresponding homogeneous foam and background-only material. The axial location of the radiation flow (here, looking at 50 eV material temperature) is seen to have a larger standard deviation for 15 μm diameter clump configurations compared to 2 μm configurations, due to there

being fewer 15 μm clumps in the domain for the same clump volume fraction. A larger computational domain size reduces the standard deviation for the 15 μm clump inhomogeneous configurations. For some inhomogeneous configurations (black lines), the plotted temperature (averaged across the width of the computational domain) near the radiation drive boundary (0 μm) is smaller due to optically thick clumps present at the boundary partially blocking radiation flow and taking a longer time to heat than the optically thin background. Future research will extend these convergence studies to larger amounts of inhomogeneous configurations, characterizing the average and standard deviations for parameters including density, radiation temperature, and the resulting spectroscopy signal.

Specific inhomogeneous configurations with known component distributions can allow experiments to validate simulations. Development of numerical methods to treat radiation flow in stochastic media can be verified and then implemented into these simulations for comparison. Detailed characterization of radiation flow is required to distinguish between models.

VII. CONCLUSION

The present research uses the Cassio code to design high energy density physics experiments for radiation flow through inhomogeneous media. Each target is an individual configuration of a probability distribution of a defined stochastic media. Spectroscopic measurements are made, simultaneously, of both the optically thin aerogel-foam background and the randomly dispersed, optically thick clumps. The inhomogeneous foam experimental platform involves a time-dependent radiation drive sending a radiation wave through the hydrodynamically-evolving material. With a large-enough size (here, larger than 10 μm diameter for a 1 μm photon mean free path) of the optically thick V_2O_5 clumps—which reduces how quickly the clumps mix with the optically thin $(Sc_2O_3)(SiO_2)_4$ background—the bulk radiation flow in inhomogeneous configurations travels faster than in homogeneous materials with equivalent amounts of component masses. This complex system challenges numerical methods for modeling radiation-hydrodynamics transport-in-stochastic-media, and this work will help validate and benchmark current and future methods and models. Detailed diagnostic measurements of radiation flow experiments with well-characterized initial conditions can discriminate between model predictions and inform how numerical methods are implemented. Ultimately, a collection of experimental results will validate ensemble-average methods and their estimated standard deviation of radiation transport through stochastic media.

Appendix A: Lineouts for Spectroscopy

The synthetic spectroscopy in Fig. 8 is generated from lineouts of the conditions of density, temperature, and materials as shown in Fig. 10.

ACKNOWLEDGMENTS

This work was supported by the U.S. Department of Energy (DOE) contract number 89233218CNA000001 for Los Alamos National Laboratory, owned by Triad National Security, LLC, for the U.S. DOE's National Nuclear Security Administration.

[1] T. Afshar-rad, M. Desselberger, M. Dunne, J. Edwards, J. M. Foster, D. Hoarty, M. W. Jones, S. J. Rose, P. A. Rosen, R. Taylor, and O. Willi, "Supersonic propagation of an ionization front in low density foam targets driven by thermal radiation," Physical Review Letters **73**, 74–77 (1994).
[2] P. A. Rosen, J. M. Foster, M. J. Taylor, P. A. Keiter, C. C. Smith, J. R. Finke, M. Gunderson, and T. S. Perry, "Experiments to study radiation transport in clumpy media," Astrophysics and Space Science **307**, 213–217 (2007).
[3] P. Keiter, M. Gunderson, J. Foster, P. Rosen, A. Comley, M. Taylor, and T. Perry, "Radiation transport in inhomogeneous media," Physics of Plasmas **15**, 056901 (2008).
[4] A. S. Moore, T. M. Guymer, J. Morton, B. Williams, J. L. Kline, N. Bazin, C. Bentley, S. Allan, K. Brent, A. J. Comley, K. Flippo, J. Cowan, J. M. Taccetti, K. Mussack-Tamashiro, D. W. Schmidt, C. E. Hamilton, K. Obrey, N. E. Lanier, J. B. Workman, and R. M. Stevenson, "Characterization of supersonic radiation diffusion waves," Journal of Quantitative Spectroscopy and Radiative Transfer **159**, 19–28 (2015).
[5] T. M. Guymer, A. S. Moore, J. Morton, J. L. Kline, S. Allan, N. Bazin, J. Benstead, C. Bentley, A. J. Comley, J. Cowan, K. Flippo, W. Garbett, C. Hamilton, N. E. Lanier, K. Mussack, K. Obrey, L. Reed, D. W. Schmidt, R. M. Stevenson, J. M. Taccetti, and J. Workman, "Quantifying equation-of-state and opacity errors using integrated supersonic diffusive radiation flow experiments on the national ignition facility," Physics of Plasmas **22**, 043303 (2015).
[6] P. Boissé, "Radiative transfer inside clumpy media-the penetration of uv photons inside molecular clouds," Astronomy and Astrophysics (ISSN 0004-6361), vol. 228, no. 2, Feb. 1990, p. 483-502. **228**, 483–502 (1990).
[7] A. Y. Poludnenko, A. Frank, and E. G. Blackman, "Hydrodynamic interaction of strong shocks with inhomogeneous media. i. adiabatic case," The Astrophysical Journal **576**, 832–848 (2002).
[8] C. L. Fryer, C. J. Fontes, J. S. Warsa, P. W. A. Roming, S. X. Coffing, and S. R. Wood, "The role of inhomogeneities in supernova shock breakout emission," The Astrophysical Journal **898**, 123 (2020).
[9] M. J. Thompson and S. Zharkov, "Recent developments in local helioseismology," Solar Physics **251**, 225–240 (2008).
[10] L. Gizon, A. C. Birch, and H. C. Spruit, "Local helioseismology: Three-dimensional imaging of the solar interior," Annual Review of Astronomy and Astrophysics **48**, 289–338 (2010).
[11] A. G. Kosovichev, "Local helioseismology of sunspots: Current status and perspectives," Solar Physics **279**, 323–348 (2012).
[12] O. Avaste and G. Vaynikko, "Solar radiation transfer in broken clouds," Academy of Sciences, USSR, Izvestiya, Atmospheric and Oceanic Physics **10**, 645–649 (1974).
[13] O. A. Avaste and G. M. Vainikko, "A Method of Calculating Radiative Transfer in Broken Clouds," in *Radiation in the Atmosphere*, edited by H. J. Bolla (1977) p. 221.

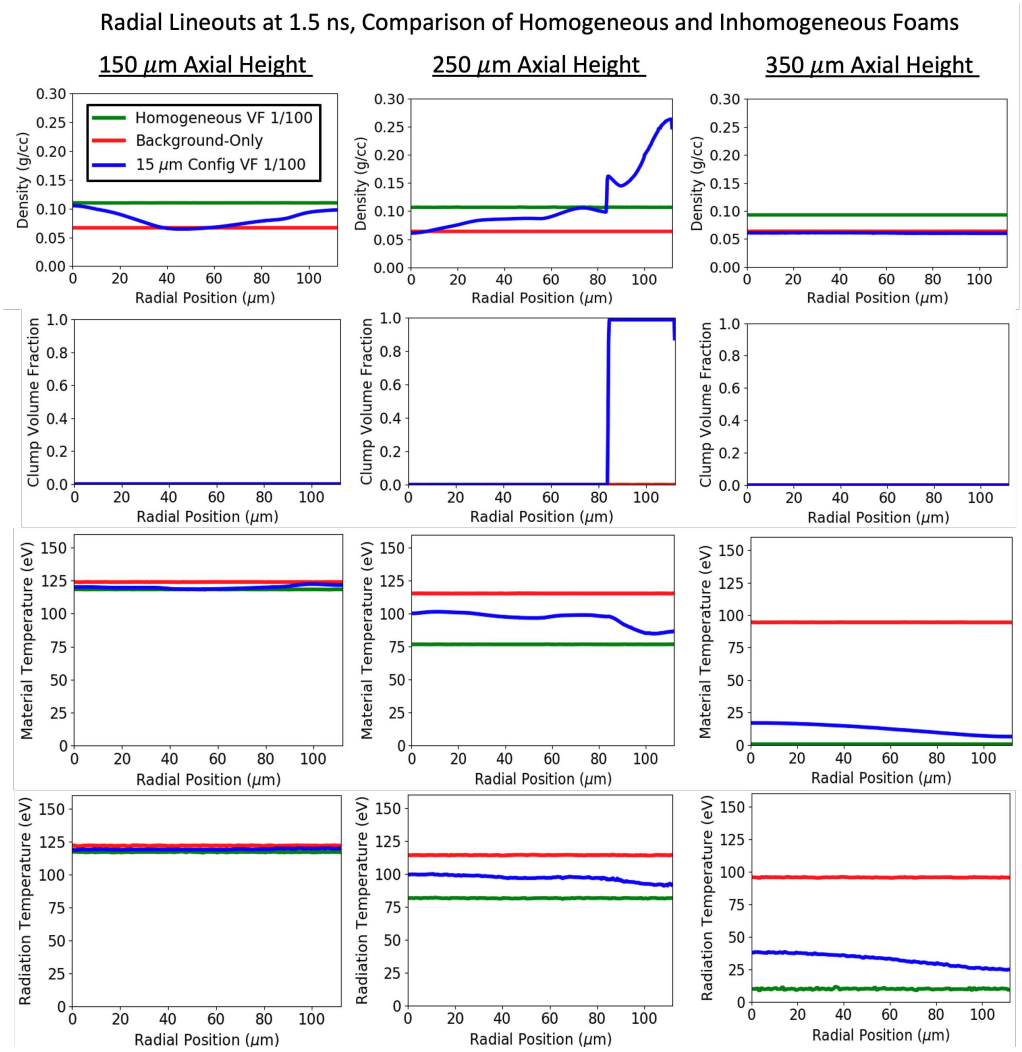

FIG. 10. Radial lineouts (along the simulation R or X direction) for density (Top Row), clump volume fraction (Second Row), material temperature (Third Row), and radiation temperature (Bottom Row) at various axial heights 150 μm (Left), 250 μm (Middle), 350 μm (Right), corresponding to the conditions that generate the spectroscopy signals in Fig. 8.

[14]E. Kassianov, T. Ackerman, R. Marchand, and M. Ovtchinnikov, "Stochastic radiative transfer in multilayer broken clouds. part ii: validation tests," Journal of Quantitative Spectroscopy and Radiative Transfer **77**, 395–416 (2003).
[15]R. Devanathan, L. V. Brutzel, A. Chartier, C. Guéneau, A. E. Mattsson, V. Tikare, T. Bartel, T. Besmann, M. Stan, and P. V. Uffelen, "Modeling and simulation of nuclear fuel materials," Energy & Environmental Science **3**, 1406 (2010).
[16]E. Merzari, P. Fischer, M. Min, S. Kerkemeier, A. Obabko, D. Shaver, H. Yuan, Y. Yu, J. Martinez, L. Brockmeyer, L. Fick, G. Busco, A. Yildiz, and Y. Hassan, "Toward exascale: Overview of large eddy simulations and direct numerical simulations of nuclear reactor flows with the spectral element method in nek5000," Nuclear Technology **206**, 1308–1324 (2020).
[17]A. R. A. Anderson and V. Quaranta, "Integrative mathematical oncology," Nature Reviews Cancer **8**, 227–234 (2008).

[18]J. K. Shultis and R. E. Faw, "Radiation shielding technology," Health Physics **88**, 297–322 (2005).
[19]M. A. Sazali, N. K. A. M. Rashid, and K. Hamzah, "A review on multilayer radiation shielding," IOP Conference Series: Materials Science and Engineering **555**, 012008 (2019).
[20]M. Pharr, W. Jakob, and G. Humphreys, *Physically based rendering: From theory to implementation* (Morgan Kaufmann, 2016).
[21]C. J. Garasi, D. E. Bliss, T. A. Mehlhorn, B. V. Oliver, A. C. Robinson, and G. S. Sarkisov, "Multi-dimensional high energy density physics modeling and simulation of wire array Z-pinch physics," Physics of Plasmas **11**, 2729–2737 (2004).
[22]J. P. Chittenden, S. V. Lebedev, C. A. Jennings, S. N. Bland, and A. Ciardi, "X-ray generation mechanisms in three-dimensional simulations of wire array Z-pinches," Plasma Physics and Controlled Fusion **46**, B457–B476 (2004).
[23]P. Tzeferacos, A. Rigby, A. Bott, A. R. Bell, R. Bingham, A. Casner, F. Cattaneo, E. M. Churazov, J. Emig, N. Flocke, F. Fiuza, C. B. Forest, J. Foster, C. Graziani, J. Katz, M. Koenig, C.-K. Li, J. Meinecke, R. Petrasso, H.-S. Park, B. A. Remington, J. S. Ross, D. Ryu, D. Ryutov, K. Weide, T. G. White, B. Reville, F. Miniati, A. A. Schekochihin, D. H. Froula, G. Gregori, and D. Q. Lamb, "Numerical modeling of laser-driven experiments aiming to demonstrate magnetic field amplification via turbulent dynamo," Physics of Plasmas **24**, 041404 (2017).
[24]B. M. Haines, R. C. Shah, J. M. Smidt, B. J. Albright, T. Cardenas, M. R. Douglas, C. Forrest, V. Y. Glebov, M. A. Gunderson, C. Hamilton, K. Henderson, Y. Kim, M. N. Lee, T. J. Murphy, J. A. Oertel, R. E. Olson, B. M. Patterson, R. B. Randolph, and D. Schmidt, "The rate of development of atomic mixing and temperature equilibration in inertial confinement fusion implosions," Physics of Plasmas **27**, 102701 (2020).
[25]A. L. Kritcher, C. V. Young, H. F. Robey, C. R. Weber, A. B. Zylstra, O. A. Hurricane, D. A. Callahan, J. E. Ralph, J. S. Ross, K. L. Baker, D. T. Casey, D. S. Clark, T. Döppner, L. Divol, M. Hohenberger, L. B. Hopkins, S. L. Pape, N. B. Meezan, A. Pak, P. K. Patel, R. Tommasini, S. J. Ali, P. A. Amendt, L. J. Atherton, B. Bachmann, D. Bailey, L. R. Benedetti, R. Betti, S. D. Bhandarkar, J. Biener, R. M. Bionta, N. W. Birge, E. J. Bond, D. K. Bradley, T. Braun, T. M. Briggs, M. W. Bruhn, P. M. Celliers, B. Chang, T. Chapman, H. Chen, C. Choate, A. R. Christopherson, J. W. Crippen, E. L. Dewald, T. R. Dittrich, M. J. Edwards, W. A. Farmer, J. E. Field, D. Fittinghoff, J. A. Frenje, J. A. Gaffney, M. G. Johnson, S. H. Glenzer, G. P. Grim, S. Haan, K. D. Hahn, G. N. Hall, B. A. Hammel, J. Harte, E. Hartouni, J. E. Heebner, V. J. Hernandez, H. Herrmann, M. C. Herrmann, D. E. Hinkel, D. D. Ho, J. P. Holder, W. W. Hsing, H. Huang, K. D. Humbird, N. Izumi, L. C. Jarrott, J. Jeet, O. Jones, G. D. Kerbel, S. M. Kerr, S. F. Khan, J. Kilkenny, Y. Kim, H. Geppert-Kleinrath, V. Geppert-Kleinrath, C. Kong, J. M. Koning, M. K. G. Kruse, J. J. Kroll, B. Kustowski, O. L. Landen, S. Langer, D. Larson, N. C. Lemos, J. D. Lindl, T. Ma, M. J. MacDonald, B. J. MacGowan, A. J. Mackinnon, S. A. MacLaren, A. G. MacPhee, M. M. Marinak, D. A. Mariscal, E. V. Marley, L. Masse, K. Meaney, P. A. Michel, M. Millot, J. L. Milovich, J. D. Moody, A. S. Moore, J. W. Morton, T. Murphy, K. Newman, J.-M. G. D. Nicola, A. Nikroo, R. Nora, M. V. Patel, L. J. Pelz, J. L. Peterson, Y. Ping, B. B. Pollock, M. Ratledge, N. G. Rice, H. Rinderknecht, M. Rosen, M. S. Rubery, J. D. Salmonson, J. Sater, S. Schiaffino, D. J. Schlossberg, M. B. Schneider, C. R. Schroeder, H. A. Scott, S. M. Sepke, K. Sequoia, M. W. Sherlock, S. Shin, V. A. Smalyuk, B. K. Spears, P. T. Springer, M. Stadermann, S. Stoupin, D. J. Strozzi, L. J. Suter, C. A. Thomas, R. P. J. Town, C. Trosseille, E. R. Tubman, P. L. Volegov, K. Widmann, C. Wild, C. H. Wilde, B. M. V. Wonterghem, D. T. Woods, B. N. Woodworth, M. Yamaguchi, S. T. Yang, and G. B. Zimmerman, "Design of inertial fusion implosions reaching the burning plasma regime," Nature Physics **18**, 251–258 (2022).
[26]J. B. Keller *et al.*, *Stochastic equations and wave propagation in random media*, Vol. 16 (American Mathematical Society Providence, RI, 1964).
[27]D. Vanderhaegen, "Radiative transfer in statistically heterogeneous mixtures," Journal of Quantitative Spectroscopy and Radiative Transfer **36**, 557–561 (1986).
[28]F. Malvagi, C. D. Levermore, and G. C. Pomraning, "Asymptotic limits of a statistical transport description," Transport Theory and Statistical Physics **18**, 287–311 (1989).
[29]G. B. Zimmerman and M. L. Adams, "Algorithms for Monte Carlo particle transport in binary statistical mixtures," Transactions of the American Nuclear Society; (United States) **63** (1991).
[30]B. Su and G. Pomraning, "Limiting correlation length solutions in stochastic radiative transfer," Journal of Quantitative Spectroscopy and Radiative Transfer **51**, 893–912 (1994).
[31]G. Pomraning, "Radiative transfer and transport phenomena in stochastic media," International Journal of Engineering Science **36**, 1595–1621 (1998).
[32]D. Miller, F. Graziani, and G. Rodrigue, "Benchmarks and models for time-dependent grey radiation transport with material temperature in binary stochastic media," Journal of Quantitative Spectroscopy and Radiative Transfer **70**, 115–128 (2001).
[33]C. Smith, "Opacity considerations for an experiment to measure radiation flow in an inhomogeneous binary mixture," Journal of Quantitative Spectroscopy and Radiative Transfer **81**, 451–459 (2003).
[34]E. Kassianov, "Stochastic radiative transfer in multilayer broken clouds. part i: Markovian approach," Journal of Quantitative Spectroscopy and Radiative Transfer **77**, 373–393 (2003).
[35]A. K. Prinja and G. L. Olson, "Grey radiative transfer in binary statistical media with material temperature coupling: asymptotic limits," Journal of Quantitative Spectroscopy and Radiative Transfer **90**, 131–159 (2005).
[36]G. L. Olson, D. S. Miller, E. W. Larsen, and J. E. Morel, "Chord length distributions in binary stochastic media in two and three dimensions," Journal of Quantitative Spectroscopy and Radiative Transfer **101**, 269–283 (2006).
[37]G. L. Olson, "Gray radiation transport in multi-dimensional stochastic binary media with material temperature coupling," Journal of Quantitative Spectroscopy and Radiative Transfer **104**, 86–98 (2007).
[38]E. W. Larsen and A. K. Prinja, "A new derivation of Akcasu's "MLP" equations for 1-D particle transport in stochastic media," Annals of Nuclear Energy **35**, 620–626 (2008).
[39]A. B. Davis and F. Xu, "A generalized linear transport model for spatially correlated stochastic media," Journal of Computational and Theoretical Transport **43**, 474–514 (2014).
[40]P. S. Brantley, N. A. Gentile, and G. B. Zimmerman, "Beyond Levermore-Pomraning for Implicit Monte Carlo radiative transfer in binary stochastic media," (LLNL-CONF-724017, 2017).
[41]C. Larmier, A. Mazzolo, A. Zoia, S. Lemaire, and D. Riz, "Preliminary investigations of transport in heterogeneous random media," EPJ Web of Conferences **247**, 04009 (2021).
[42]C. D. Levermore, G. C. Pomraning, D. L. Sanzo, and J. Wong, "Linear transport theory in a random medium," Journal of Mathematical Physics **27**, 2526–2536 (1986).
[43]O. A. Hurricane and J. H. Hammer, "Bent marshak waves," Physics of Plasmas **13**, 113303 (2006).
[44]F. W. Doss, "Exact results on intrinsic gradients in the compression of heat," (American Nuclear Society, 2021) pp. 1134–1142.
[45]E. Malka and S. I. Heizler, "Supersonic–subsonic transition region in radiative heat flow via self-similar solutions," Physics of Fluids **34**, 066105 (2022).
[46]J. M. Taccetti, P. A. Keiter, N. Lanier, K. Mussack, K. Belle, and G. R. Magelssen, "A technique for measuring the propagation of a supersonic radiation front in foam via spatially resolved spectral imaging of a tracer layer," Review of Scientific Instruments **83**, 023506 (2012).
[47]B. M. Patterson and C. E. Hamilton, "Dimensional standard for micro x-ray computed tomography," Analytical Chemistry **82**,

8537–8543 (2010).
[48]C. Fryer, A. Diaw, C. Fontes, A. Hungerford, J. Kline, H. Johns, N. Lanier, S. Wood, and T. Urbatsch, "Designing radiation transport tests: Simulation-driven uncertainty-quantification of the coax temperature diagnostic," High Energy Density Physics **35**, 100738 (2020).
[49]H. Johns, C. Fryer, S. Wood, C. Fontes, P. Kozlowski, N. Lanier, A. Liao, T. Perry, J. Morton, C. Brown, D. Schmidt, T. Cardenas, T. Urbatsch, P. Hakel, J. Colgan, S. Coffing, J. Cowan, D. Capelli, L. Goodwin, T. Quintana, C. Hamilton, F. Fierro, C. Wilson, R. Randolph, P. Donovan, T. Sedillo, R. Gonzales, M. Sherrill, M. Douglas, W. Garbett, J. Hager, and J. Kline, "A temperature profile diagnostic for radiation waves on OMEGA-60," High Energy Density Physics **39**, 100939 (2021).
[50]S. X. Coffing, C. L. Fryer, H. F. Robey, C. J. Fontes, S. R. Wood, P. M. Kozlowski, H. M. Johns, D. D. Meyerhofer, T. Byvank, A. Liao, and T. J. Urbatsch, "Inferring the temperature profile of the radiative shock in the COAX experiment with shock radiography, Dante, and spectral temperature diagnostics," Physics of Plasmas **29**, 083302 (2022).
[51]C. Fryer, S. Wood, S. Coffing, H. Robey, C. Fontes, H. Johns, P. Kozlowski, T. Urbatsch, N. Lanier, D. Meyerhofer, and T. Byvank, "Detailed temperature diagnostic studies for radishock and coax experiments," High Energy Density Physics **46**, 101023 (2023).
[52]C. E. Hamilton, D. Honnell, B. M. Patterson, D. W. Schmidt, and K. A. D. Obrey, "Incorporation of tracer elements within aerogels and ch foams," Fusion Science and Technology **59**, 194–198 (2011).
[53]R. B. Randolph, J. A. Oertel, T. Cardenas, C. E. Hamilton, D. W. Schmidt, B. M. Patterson, F. Fierro, and D. Capelli, "Dry-machining of aerogel foams, ch foams, and specially engineered foams using turn-milling techniques," Fusion Science and Technology **73**, 187–193 (2018).
[54]C. Fryer, E. Dodd, W. Even, C. Fontes, C. Greeff, A. Hungerford, J. Kline, K. Mussack, I. Tregillis, J. Workman, J. Benstead, T. Guymer, A. Moore, and J. Morton, "Uncertainties in radiation flow experiments," High Energy Density Physics **18**, 45–54 (2016).
[55]A. Y. Poludnenko, K. K. Dannenberg, R. P. Drake, A. Frank, J. Knauer, D. D. Meyerhofer, M. Furnish, J. R. Asay, and S. Mitran, "A laboratory investigation of supersonic clumpy flows: Experimental design and theoretical analysis," The Astrophysical Journal **604**, 213–221 (2004).
[56]R. F. Coker, B. H. Wilde, J. M. Foster, B. E. Blue, P. A. Rosen, R. J. R. Williams, P. Hartigan, A. Frank, and C. A. Back, "Numerical simulations and astrophysical applications of laboratory jets at Omega," Astrophysics and Space Science **307**, 57–62 (2007).
[57]P. A. Rosen, J. M. Foster, B. H. Wilde, P. Hartigan, B. E. Blue, J. F. Hansen, C. Sorce, R. J. R. Williams, R. Coker, and A. Frank, "Laboratory experiments to study supersonic astrophysical flows interacting with clumpy environments," Astrophysics and Space Science **322**, 101–105 (2009).
[58]M. Gittings, R. Weaver, M. Clover, T. Betlach, N. Byrne, R. Coker, E. Dendy, R. Hueckstaedt, K. New, W. R. Oakes, D. Ranta, and R. Stefan, "The rage radiation-hydrodynamic code," Computational Science I& Discovery **1**, 015005 (2008).
[59]J. Wohlbier, C. Wingate, T. Masser, G. Bowers, and M. Sorice, "Plans for and progress towards and inertial confinement fusion code from the crestone project," (2007) p. BP8.035.
[60]J. Colgan, D. P. Kilcrease, N. H. Magee, M. E. Sherrill, J. Abdallah, Jr., P. Hakel, C. J. Fontes, J. A. Guzik, and K. A. Mussack, "A New Generation of Los Alamos Opacity Tables," **817**, 116 (2016).
[61]P. Hakel, M. Sherrill, S. Mazevet, J. Abdallah, J. Colgan, D. Kilcrease, N. Magee, C. Fontes, and H. Zhang, "The new Los Alamos opacity code ATOMIC," Journal of Quantitative Spectroscopy and Radiative Transfer **99**, 265–271 (2006).
[62]C. J. Fontes, H. L. Zhang, J. Abdallah, J., R. E. H. Clark, D. P. Kilcrease, J. Colgan, R. T. Cunningham, P. Hakel, N. H. Magee, and M. E. Sherrill, "The Los Alamos suite of relativistic atomic physics codes," Journal of Physics B Atomic Molecular Physics **48**, 144014 (2015).
[63]M. Simmons, P. Langston, and A. Burbidge, "Particle and droplet size analysis from chord distributions," Powder Technology **102**, 75–83 (1999).
[64]E. I. Moses, R. E. Bonanno, C. A. Haynam, R. L. Kauffman, B. J. MacGowan, R. W. Patterson, R. H. Sawicki, and B. M. V. Wonterghem, "The national ignition facility: path to ignition in the laboratory," The European Physical Journal D **44**, 215–218 (2007).
[65]H. M. Johns, T. Byvank, H. Robey, T. Urbatsch, S. Coffing, C. L. Fryer, T. S. Perry, P. M. Kozlowski, C. J. Fontes, K. Love, D. D. Meyerhofer, E. S. Dodd, Y. P. Opachich, L. Kot, R. F. Heeter, and S. Finnegan, "Roadmap for the exposé of radiation flows (Xflows) experiment on NIF," Review of Scientific Instruments **94**, 023502 (2023).